Influence of Collimator Characteristics on Quantification in SPECT

John S. Fleming and Abdulaziz S. Alaamer
Department of Medical Physics and Bio-Engineering, Southampton General Hospital, Southampton, England

Accurate, absolute quantification of activity in SPECT depends on the counting sensitivity of the gamma camera collimator system and on the contribution of the tail of the point spread function (PSF) that contains both scattered radiation and septal penetration. **Methods:** These factors were studied for the radionuclides ^{99m}Tc, ^{131}I and ^{123}I on different cameras and collimators. The ability of the geometric mean line source scatter function subtraction technique to correct for the effect of the tail of the PSF was investigated in a computer simulation study with ^{99m}Tc and a physical phantom study with ^{123}I. **Results:** The sensitivities of ^{99m}Tc collimators were relatively constant with distance in air whereas those of ^{123}I and ^{131}I decreased considerably. For these radionuclides the contribution of the PSF tail was also increased as compared to ^{99m}Tc. The geometric mean line source scatter function subtraction technique was confirmed as being able to correct effectively for this factor. **Conclusion:** Collimator design affects both the fall off of sensitivity in air and the tail of the PSF. Attention to correction of these factors enables accurate quantification.

Key Words: SPECT; quantitative measurements; collimator characteristics

J Nucl Med 1996; 37:1832–1836

Accurate absolute quantification of activity in SPECT is valuable in increasing the information available in both clinical routine (*1*) and research (*2*) applications. A recent review highlighted the value of quantification and the requirement of attention to detail in the methodology (*3*). Quantification depends critically on knowledge of the sensitivity of the camera collimator system in counts per second per megabecquerel (*4*). Sensitivity is usually assumed to be independent of distance from the collimator. Although this is generally true for many low-energy collimators with ^{99m}Tc, it has been shown previously to be invalid for ^{131}I (*5*).

Another important factor in quantification is the ability to deal with incorrectly positioned scattered photons. A successful method of dealing with this problem is the use of the geometric mean scatter function. This is measured by fitting the tail of either the geometric mean line-source function or point-source function to an exponential function (*5–7*). Convolution of the scatter function with the projection image data produces an estimate of the scatter contribution to the image. This can be subtracted from the geometric mean projection data to correct for scatter. The accuracy of this procedure can be refined by iteration (*8*). One of the advantages of this approach is that it also deals with other contributions to the tail of the line or point spread function such as septal penetration. This is particularly important for radionuclides with high-energy gamma emission, either in their own decay scheme or due to impurities. The tail of the line spread function is referred to as the scatter function, although it also contains a septal penetration component (*5*).

Received Sept. 21, 1995; revision accepted Jan. 24, 1996.
For correspondence or reprints contact: Dr. J.S. Fleming, Department of Nuclear Medicine, Southampton General Hospital, Southampton SO16 6YD, U.K.

The variation of sensitivity with distance from the collimator in air and the geometric mean-line source scatter function are measured and compared for ^{99m}Tc, ^{131}I and ^{123}I on two gamma cameras. The influence of energy window, source depth and line length on scatter function also is studied. The geometric mean line source scatter function subtraction technique for scatter and septal penetration correction has been validated for ^{99m}Tc and ^{131}I (*4,5,7,8*). New data are presented on the validation of the technique for ^{123}I in a physical phantom study. To investigate error sources due to the algorithm alone, the technique is also assessed for its ability to quantify the activity of objects containing ^{99m}Tc in a computer simulation experiment.

MATERIALS AND METHODS

Measurement of Sensitivity and Scatter Function

A few megabecquerels of radionuclide were measured in an isotope calibrator and introduced to an acrylic phantom of 6 × 6 × 1 cm. This was placed beneath the gamma camera and the distance from the collimator measured. An image of the phantom of 10^5 counts was acquired in the computer and the duration of imaging noted. The counting rates obtained were sufficiently low for dead time effects on the measurements to be ignored. For ^{99m}Tc, the total count in the image was used to assess sensitivity. However, for ^{131}I and ^{123}I, there was a relatively large contribution to the total count in areas remote from the source and a consistent operator-independent method of outlining the source alone was required. The method used in this study was to smooth the image twice (using a 9-point smooth with 1:2:4 weighting) and outline the phantom with a contour at 20% of the maximum count.

The procedure was repeated with distances in air from the collimator varying between 0 and 30 cm. An image of natural background radiation was also acquired and the count subtracted from that of the phantom. The sensitivity measurement was performed for ^{99m}Tc, ^{131}I and ^{123}I on two gamma cameras: an International General Electric 400AT (International General Electric Co., New York) (Camera 1) and an ADAC Genesys (ADAC Laboratories, Milpitas, CA) (Camera 2). Low-energy, general-purpose collimators were used for the ^{99m}Tc and ^{123}I measurements and a high-energy, general-purpose collimator for ^{131}I. Both cameras were set with the energy windows used in clinical practice in our department, i.e. 130–160 keV for ^{99m}Tc, 350–420 keV for ^{131}I and 144–176 keV for ^{123}I. The offset windows for ^{99m}Tc and ^{131}I were used to reduce the scatter contribution. The measurement on the surface of the collimator was repeated on subsequent days to investigate the variability of sensitivity with time.

The method used for scatter function measurement was essentially that described by Axelsson et al. (*6*). A line source consisting of a thin tube, 7.5 cm long, filled with radionuclide, was suspended in a cuboid water pool phantom 20 cm deep and 30 cm wide. The source was placed at a depth of 6.8 cm and two planar images were acquired with the camera aligned horizontally above and below the source, respectively, at a radius of rotation of 22 cm. The natural

background contribution was subtracted from both images. A 5-cm wide, centrally placed horizontal profile was formed perpendicular to the line. The tail of the line spread function, between 5 and 15 cm from the line, was fitted by least squares regression to either a mono- or biexponential function as judged by subjective visual inspection of a log-linear plot of the curve. The exponential fit was assumed to describe the scatter function over all distances from zero to infinity. The experiment was performed using ^{99m}Tc and ^{123}I on both cameras with a low-energy, general-purpose collimator and ^{131}I with a high-energy collimator.

The geometric mean scatter function was also measured on Camera 2 for ^{99m}Tc with a symmetrical window (125–155 keV) to enable study of its dependence on energy window. The effect of the length of line on the scatter function was also studied on Camera 2 using measurements on lines of lengths 12 cm and 25 cm. The variation of the geometric mean scatter function with depth of the line in attenuating medium was studied for Camera 1 using the 7.5-cm line at a variety of depths.

Evaluation of the Geometric Mean Line Source Scatter Function Subtraction Technique with Iodine-123

The use of the geometric mean line source scatter function subtraction technique to quantify volume and activity of objects in SPECT imaging in phantoms containing ^{99m}Tc and ^{131}I has been described (*4,5,9*). Evaluation with ^{123}I is presented in this article. Two plastic bottles (160 ml and 300 ml containing activities of 4.7 and 6.5 MBq, respectively) were placed in a cylindrical acrylic phantom (21 cm internal diameter) filled with water. SPECT acquisition was performed on Camera 2 with 64 images around 360° at 128 × 128 matrix size. The pixel dimension was 0.467 cm. The images were reconstructed using an iterative attenuated projector-back projector algorithm in which scatter was subtracted using the geometric mean line source scatter function subtraction technique before reconstruction (*8*). The reconstructed images were scaled to read in absolute units (Bq) using a sensitivity value obtained in air at the radius of rotation.

The volumes of the bottles were evaluated using a threshold determined by maximization of interclass variance (*4*). This method selected the threshold that optimally separated voxels within objects containing activity from their surroundings. Systematic errors in volume estimation were corrected using the previously obtained regression equation between true and measured values of volume (*4*). The volume defined by the threshold was then dilated by three pixels (14.1 mm) to include all the counts due to the object. The activity in the object was then calculated by summing the activity in the dilated volume and correcting for systematic error as described above.

Evaluation of the Geometric Mean Line Source Scatter Function Subtraction Technique with Technetium-99m by Computer Simulation

The quantitative accuracy of the technique was also evaluated for ^{99m}Tc in a computer simulation experiment. This test was performed as it allowed errors introduced by the algorithm to be studied in the absence of the experimental errors that are inevitably present in physical phantom measurements. The simulation program required as input definition of a three-dimensional distribution of activity and the corresponding attenuation map of the distribution volume and its surroundings. A set of 64 projection images around 360° were then simulated. The effect of each voxel containing activity on each projection image was calculated from the sum of the primary photon and scattered photon point spread functions at that position. These sums were determined as described by Fleming and Simpson (*10*) based on measurements of these functions for ^{99m}Tc on an ADAC Genesys gamma camera. The projection image was then formed by summing the contributions of all voxels containing activity. The resultant images had a matrix size of 128 by 128 with pixel dimension 4.67 mm.

TABLE 1
Mean and Standard Deviation Collimator Surface Sensitivities cps/MBq and Scatter Fractions* for ^{99m}Tc ^{123}I and ^{131}I for Both Cameras Studied

Parameter	^{99m}Tc	^{123}I	^{131}I
Sensitivity			
Camera 1	153.0 ± 2.1	117.1	69.0 ± 1.1
Camera 2	120.2 ± 1.3	124.8	40.6 ± 1.1
Scatter fraction			
Camera 1	0.063	0.115	0.302
Camera 2	0.154	0.257	0.192

*Defined as the scatter contribution in the line spread function as a fraction of total counts.

Ten objects of different volumes (range 5 to 1000 ml) containing different uniformly distributed activities of ^{99m}Tc (range 1 to 40 MBq) were simulated. The objects were contained within a water-filled cylinder of 21 cm in diameter. It should be noted that, as this simulation uses a scatter function that varies in depth but is circularly symmetric in the image plane, it does not fully test the ability of the scatter subtraction to deal with asymmetrical scatter. However, it does enable study of the effect of using a line scatter function to deal with varying out-of-plane scatter and a single-scatter function to cope with depth-dependent scatter.

RESULTS

The surface sensitivities for all radionuclides on both cameras are shown in Table 1. The variations of sensitivity in air with distance from the collimator for ^{99m}Tc and ^{123}I are illustrated in Figure 1. For Camera 1, the sensitivity for ^{99m}Tc showed a small increase with depth in air while, for Camera 2, it fell slowly with the maximum decrease compared to that on the surface being 4.1%. For both cameras fitted with low-energy collimators, the sensitivity for ^{123}I initially decreased relatively rapidly with distance from the collimator, followed by a slower decrease at higher distance values. The fall of counting rate was more marked for Camera 2 than for Camera 1, with the sensitivities at 25 cm being, respectively, 64% and 82% of the surface value. The pattern of sensitivity reduction with distance for ^{131}I was similar to that for ^{123}I with values at 25 cm for Cameras 1 and 2 being 58% and 70%, respectively.

The scatter functions for ^{99m}Tc and ^{123}I for both cameras with low-energy collimator are shown in Figure 2. The scatter functions could be fitted adequately by a monoexponential

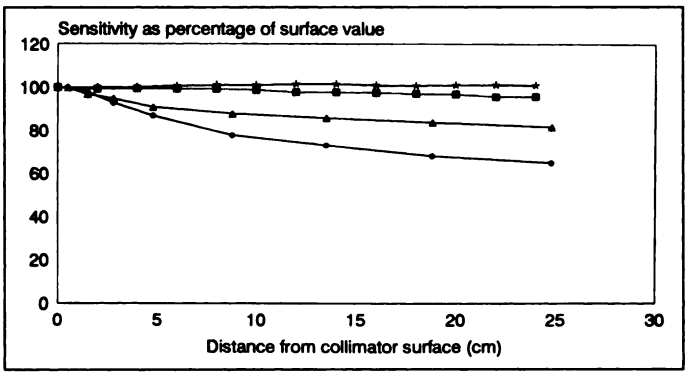

FIGURE 1. Variation with distance from collimator surface in air of the sensitivity of the gamma camera/collimator system for Cameras 1 and 2 with a low-energy, general-purpose collimator for ^{99m}Tc (* and ■, respectively) and ^{123}I (▲ and ●, respectively).

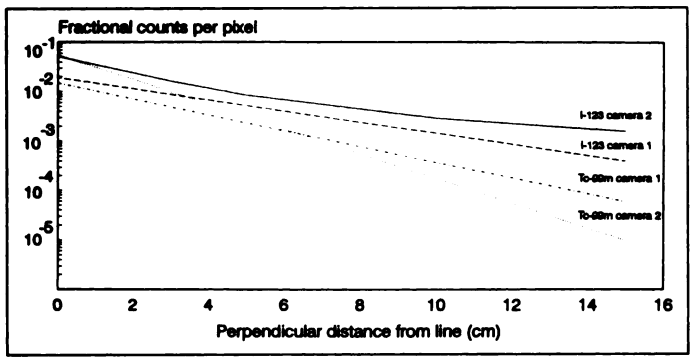

FIGURE 2. Geometric mean scatter functions for Cameras 1 and 2 for ^{99m}Tc and ^{123}I. Units of the scatter function are counts per pixel expressed as a fraction of the total count in the line spread function for a pixel size of 6.4 mm.

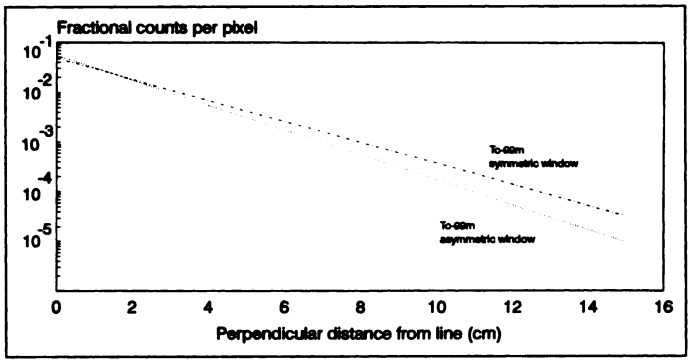

FIGURE 4. Geometric mean scatter functions for ^{99m}Tc on Camera 2 using symmetric and asymmetric energy windows. Units of the scatter function are counts per pixel expressed as a fraction of the total count in the line spread function for a pixel size of 6.4 mm.

function with the exception of ^{123}I on Camera 2 which required a biexponential fit. The area under each curve from distance zero to infinity was also calculated. This was defined as the scatter fraction and gave a measure of the total scatter contribution in the line source function as a fraction of the total counts measured. The scatter fractions for all radionuclides are shown in Table 1. For both cameras, the scatter fraction was greater for ^{123}I compared to ^{99m}Tc and for both radionuclides it was higher for Camera 2 than for Camera 1. The scatter functions for ^{131}I for both cameras fitted with high-energy collimators are shown in Figure 3. For Camera 1, there is more scatter for ^{131}I than ^{123}I, while the reverse is true for Camera 2.

The results of comparing symmetrical and asymmetrical windows for Camera 2 are shown in Figure 4. Over the measured range, the symmetrical window had a greater scatter contribution. However, the scatter fractions were estimated at 0.15 for both situations. The effect of line source length on the scatter function for ^{99m}Tc on Camera 2 is illustrated in Figure 5. The scatter fractions for lines of length 7.5, 12 and 25 cm were 0.15, 0.22 and 0.23, respectively. The scatter fraction increased significantly between line lengths of 7.5 and 12 cm but thereafter changed much more slowly. The line spread functions at different positions along the length of the 7.5-cm line source were found to show only very small differences. The depth dependence of the scatter function is shown in Figure 6. It was lowest when the line source was close to one surface of the water and highest with the line at a depth of half the total water thickness.

The results of the measurement of volume and activity in the two objects containing ^{123}I showed mean errors of 10 ml and 0.17 MBq, respectively. These errors were typical of those found when using the same technique with ^{99m}Tc and ^{131}I (*4*).

The activities of 10 objects in the simulation experiment with ^{99m}Tc were assessed with a mean underestimate of 0.5% that was not significantly different from zero. The precision of measurement was 4.0% compared to that in a similar physical phantom experiment of 4.8% (*4*).

DISCUSSION

In many applications of SPECT, the information is enhanced by quantification. Determination of the relationship between counts and activity and the subtraction of the contributions of scatter and septal penetration are key factors in obtaining the best results. Most techniques assume that sensitivity is constant with depth in air. This study confirms that for ^{99m}Tc this is essentially true, with both cameras studied having variations of less than 5% up to 25 cm from the collimator. For ^{123}I, however, the variation is larger with reductions in sensitivity up to 36%. This results from its high-energy gamma emissions that penetrate through the collimator septa particularly with low-energy collimators. Some of these photons fall in the energy window being used. This component of the counting rate reduces with distance from the collimator due to the reduced solid angle subtended at the detector.

Sensitivity measurement is vital in any assessment of absolute uptake. The value obtained depends on: (a) the accuracy of measuring the gamma camera standard activity in the isotope calibrator, (b) the relation of the energy window to the photopeak, (c) the size and shape of the standard phantom, (d) the distance of the phantom from the camera and (e) the protocol for selecting the region representing it. The variation of gamma camera standard activity measurement in the isotope calibrator may be reduced by ensuring consistent counting geometry and additional measurement of a long-lived calibrator standard. The

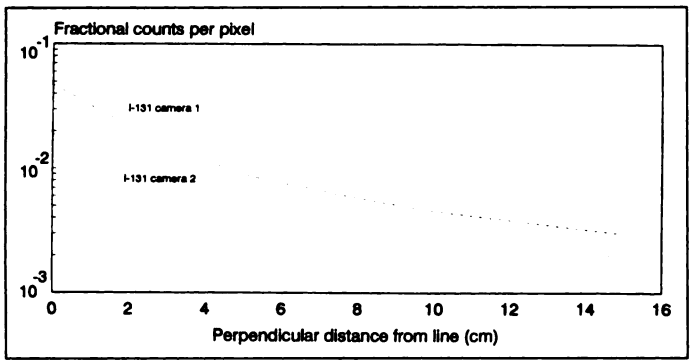

FIGURE 3. Geometric mean scatter function for ^{131}I for both cameras. Units of the scatter function are counts per pixel expressed as a fraction of the total count in the line spread function for a pixel size of 6.4 mm.

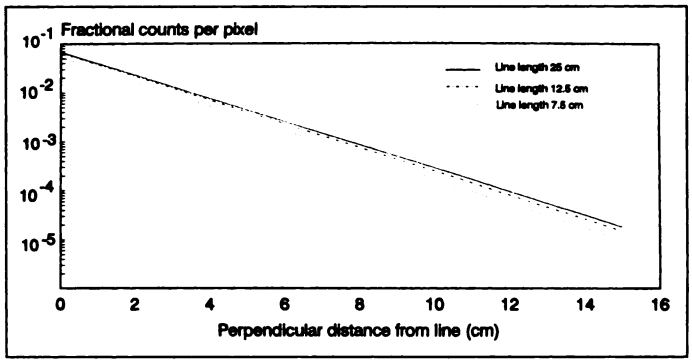

FIGURE 5. Geometric mean scatter functions of ^{99m}Tc on Camera 2 for varying lengths of line. Units of the scatter function are counts per pixel expressed as a fraction of the total count in the line spread function for a pixel size of 6.4 mm.

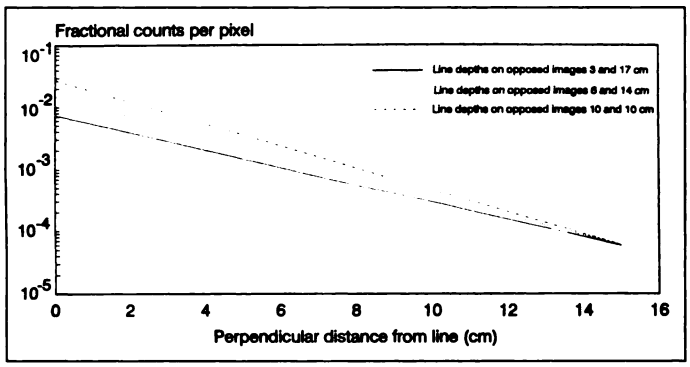

FIGURE 6. Geometric mean scatter function for ^{99m}Tc on Camera 1 for different source depths. Units of the scatter function are counts per pixel expressed as a fraction of the total count in the line spread function for a pixel size of 6.4 mm. Corresponding scatter fractions moving from the peripherally to the centrally placed line were 0.036, 0.068 and 0.105, respectively.

measurement of the gamma camera standard on the camera should also use a consistent protocol. Daily adjustment on the position of the energy window with respect to the photopeak should help minimize this cause of variability. A fixed distance should be used when assessing sensitivity, particularly for radionuclides with high-energy emissions. The low day to day variation in sensitivity observed suggests that a long-term average value may be more appropriate than a single value obtained on a particular day. A standard measurement should still be performed daily for quality control. Attenuation in the phantom and the size of the region representing it, will result in small systematic errors. It is considered reasonable not to attempt individual correction of these errors but to allow for their effect in a correction for overall systematic error (*4*).

The geometric mean line source scatter function subtraction technique requires assessment of the scatter function and this article has examined some of its dependent factors. It was first found to depend on the radionuclide used. For both cameras with a low-energy collimator, the scatter functions were higher for ^{123}I than for ^{99m}Tc. Given the similarity of the energies of the radionuclides this cannot be explained by differences in the amount of scattered radiation. The higher tail of the ^{123}I scatter function is principally due to the septal penetration of its low abundance higher energy gamma emissions. The different scatter functions found for a given radionuclide on the two cameras is mainly due to the difference in collimator characteristics. Even for ^{99m}Tc, where only septal penetration due to the principal radiation is present, there was a difference between the two low-energy collimators studied. The collimator on Camera 2 handled septal penetration less well than that on Camera 1, giving higher scatter fractions for both ^{99m}Tc and ^{123}I. The scatter function for ^{123}I could be reduced by using a higher energy collimator but at the expense of both resolution and sensitivity. The scatter fractions were on average higher for ^{131}I than for ^{123}I as might be expected from a radionuclide with a higher principal energy in addition to low abundance radiation at higher energy. In this case, the collimator of Camera 2 dealt better with septal penetration than that on Camera 1.

The scatter function was affected by the energy window used, with a symmetrical window giving larger values over the range of distances measured than a window of the same width offset at a slightly higher energy. However, the calculated scatter fractions were equal. This was probably due to the extrapolation of the monoexponential curves back to zero distance not being valid. This had been observed in a previous experiment on point source scatter functions (*10*).

The scatter function for a line source depends on the length of the line, although the variation observed was not large. Line scatter functions also vary along the length of the line being slightly greater at the center than near the edge. This was shown to be a minimal effect and, therefore, it is considered acceptable to integrate the function along the length of the line. A further approximation in using a line source function is in the oversubtraction of scatter resulting from small objects where there is little out-of-plane activity. The net effect of all these factors on quantification of activity in objects was studied in the simulation experiment. This included activity assessment in a wide range of object sizes with variable out-of-plane activity. The low random error obtained indicated that the approximations resulting from use of the line source had an acceptably small effect on quantification.

All techniques relying on a single geometric mean scatter function suffer from the fact that the geometric mean scatter contribution varies with depth (Fig. 6). The higher geometric mean scatter function at central depths is expected from studies of point source scatter that show a maximum at around 8–10 cm (*10*). The measurements made with the source at about one third of the total depth provided an effective mean scatter function. Interestingly, this is also typical of the depth of many of the organs studied by nuclear medicine techniques (*6*). The variation of scatter function with depth was included in the simulation experiment and the results indicate that the assumption of depth independence of the scatter function in scatter subtraction leads to only small errors in activity quantification. The similarity of the precision of activity measurement in the computer simulation study and that in the equivalent physical phantom study indicated the adequacy of the model used in the simulation. It also showed that asymmetry of the scatter function, that was not modeled in the simulation experiment had only a small effect on activity quantification.

Corrections for both sensitivity variation in air and scatter using the techniques described are approximations and a small systematic error is to be expected. The very low value found in the simulation experiment (0.5%) is considered somewhat fortuitous. In a previous physical phantom study using ^{131}I and ^{99m}Tc the mean systematic error was 3.0%. In practical application of the technique we would, therefore, recommend initial phantom experiments on objects of known activity to validate the technique and assess the residual systematic errors that can then be corrected in subsequent measurements.

CONCLUSION

The geometric mean line source scatter technique can provide accurate and precise quantification of activity of objects using a variety of radionuclides. Careful calibration of the sensitivity and scatter characteristics of the particular collimator used is required for accurate results.

ACKNOWLEDGMENTS

We thank the Saudi National Guard for their support of Abdulazziz Alaamer.

REFERENCES

1. Blake GM, Lewington VJ, Fleming JS, et al. Modification by nifedipine of [^{131}I] MIBG kinetics in malignant phaeochromocytoma. *Eur J Nucl Med* 1988;14:345–348.
2. Perring S, Summers Q, Fleming JS, et al. A new method of quantification of the pulmonary regional distribution of aerosols using combined CT and SPECT and its application to nedocromil sodium administered by metered dose inhaler. *Br J Radiol* 1994;67:46–53.
3. Rosenthal MS, Cullom J, Hawkins W, et al. Quantitative SPECT imaging: a review and recommendations by the Focus Committee of the Society of Nuclear Medicine Computer and Instrumentation Council. *J Nucl Med* 1995;36:1489–1513.
4. Alaamer AS, Fleming JS, Perring S. Evaluation of a technique for the quantification of radioactivity and volume of an object in SPECT. *Nucl Med Commun* 1993;14:1061–1070.

5. Fleming JS, Alaamer AS, Perring S. A technique for the absolute quantification of ^{131}I radiopharmaceuticals using SPECT. *Nucl Med Commun* 1993;14:498–505.
6. Axelsson B, Msaki P, Israelsson A. Subtraction of Compton scattered photons in SPECT. *J Nucl Med* 1984;25:490–494.
7. Msaki P, Axelsson B, Dahl CM, Larsson S. Generalized scatter correction method in SPECT using point scatter distribution functions. *J Nucl Med* 1987;28:1861–1869.
8. Fleming JS. A technique for using CT images in attenuation correction and quantification in SPECT. *Nucl Med Commun* 1989;10:83–97.
9. Alaamer AS, Fleming JS, Perring S. Evaluation of the factors affecting the accuracy and precision of a technique for quantification of volume and activity in SPECT. *Nucl Med Commun* 1994;15:758–771.
10. Fleming JS, Simpson DE. A technique for simulation of the point spread function of a gamma camera. *Phys Med Biol* 1994;39:1457–1473.

Metabolic Fate of Iodine-123-BMIPP in Canine Myocardium after Administration of Etomoxir

Ryohei Hosokawa, Ryuji Nohara, Yasuhisa Fujibayashi, Kazumi Okuda, Motonari Ogino, Tatsuhiko Hata, Masatoshi Fujita, Nagara Tamaki, Junji Konishi and Shigetake Sasayama

Third Division, Department of Internal Medicine and Department of Nuclear Medicine, Kyoto University Hospital and Department of Genetic Biochemistry, Faculty of Pharmaceutical Sciences, Kyoto University, Kyoto, Japan

To clarify the metabolic fate of ^{123}I-(-p-iodophenyl)-3-R,S-methylpentadecanoic acid (BMIPP) in dysfunctional myocardium, a comparison between normal dogs and those with etomoxir administration was studied using an open-chest canine model. **Methods:** Using open-chested dogs under anesthesia, we created a system to release all the blood in the great cardiac vein outside without recirculation, if necessary. Iodine-123-BMIPP was directly injected into the left anterior descending artery, its extraction, retention and washout rate in the early phase were calculated, and the metabolites in the myocardium were evaluated using a high-performance liquid chromatography. Moreover, these factors were compared between normal dogs and those pretreated with etomoxir, that creates a condition similar to ischemia. **Results:** Although rapid extraction of BMIPP from the plasma into the myocardium and the subsequent retention were unchanged, early washout (8 min) of radioactivity significantly increased (49.6%±13.3% → 70.5%±10.7%, $p < 0.05$) with etomoxir. The levels of the full metabolite formed by complete oxidation of BMIPP decreased significantly with etomoxir (21.4%±10.9% → 5.5%±3.5%, $p < 0.01$). In addition, back diffusion of BMIPP increased (25.1%±8.0%→41.9%±12.0%, $p < 0.05$) in the etomoxir-treated animals without affecting the levels of alpha-oxidation metabolite and the intermediate metabolites. **Conclusion:** BMIPP is very sensitive to etomoxir and is suitable for assessing mitochondrial dysfunction. Iodine-123-BMIPP might be a promising radiopharmaceutical for the evaluation of ischemic heart disease, cardiomyopathy and mitochondrial encephalomyopathy.

Key Words: fatty acid metabolism; BMIPP; etomoxir; mitochondrial function

J Nucl Med 1996; 37:1836–1840

Iodine-123-(ρ-iodophenyl)-3-R,S-methylpentadecanoic acid (^{123}I-BMIPP) is a radioiodinated fatty acid analog in which a methyl group has been introduced into the beta (3) position of the fatty acid chain to inhibit rapid myocardial catabolism (*1,2*). Therefore, BMIPP has a long retention in the myocardium by incorporation into the triglyceride pool (*3,4*) and good characteristics for clinical SPECT imaging. Clinical protocols using BMIPP have been performed at several institutions in western Europe (*5–8*) and Japan (*9–11*) to evaluate impairment of myocardial fatty acid metabolism and myocardial viability. Although ^{123}I-BMIPP is now widely used in Japan as an approved radiopharmaceutical and studies with more than 50,000 patients have been completed (Yamada H, *unpublished data*, 1995), the metabolic fate and pathway for catabolism of BMIPP in the myocardium are still not completely elucidated. However, this agent does not show ideal irreversible retention like the ^{123m}Te-containing fatty acids (*12*) or beta-dimethyl substituted fatty acids (*3*), and a part of BMIPP is metabolized through alpha-oxidation followed by beta-oxidation to small catabolites in a recirculating isolated rat heart (*13*).

In our previous study using open-chested canines and analysis with high-performance liquid chromatography (HPLC), myocardial metabolism of BMIPP in normal dogs was studied (*14*), and BMIPP was found to be well retained in the myocardium and to have the same metabolic fate as observed with BMIPP administered to isolated rat hearts (*13*). Still to be clarified, however, is how alpha- and beta-oxidation, and/or backdiffusion of nonmetabolized BMIPP might contribute to the washout of BMIPP from dysfunctional myocardium such as ischemic heart disease or cardiomyopathy.

The aim of this study is to evaluate myocardial metabolism of BMIPP with etomoxir, which creates a condition similar to ischemia, and to assess the potential usefulness of BMIPP for ischemic heart disease, cardiomyopathy and mitochondrial encephalomyopathy.

MATERIALS AND METHODS

Iodine-123-BMIPP and standard samples for HPLC were generously donated by the Nihon Medi-physics Co. Ltd. (Tokyo, Japan). Iodine-125-bovine serum albumin (^{125}I-BSA) was prepared by the conventional chloramine T method. Etomoxir was obtained from ASAT AG (Zug, Switzerland).

Surgical Preparation

The surgical preparation is illustrated in Figure 1, which followed the method previously reported (*15*) with some modifications. After overnight fasting, male mongrel dogs, weighing 18.5–32.0 kg, received an intramuscular injection of ketalar (2.5 mg/kg) for induction of anesthesia and an intravenous injection of pentobarbital (25 mg/kg) for its maintenance. For respiration, an endotracheal tube was connected to a dual-phase control respirator through which 100% 2l/min oxygen was supplied. The fifth intercostal space was opened and the epicardium was immobilized in the form of a cradle. The left anterior descending artery (LAD) was dissected free for radioisotope administration, and the great

Received Oct. 24, 1995; revision accepted March 20, 1996.
For correspondence or reprints contact: Ryuji Nohara, MD, Third Division, Department of Internal Medicine, Kyoto University Hospital, 54 Kawaracho, Shogoin, Sakyoku, Kyoto City, 606 Japan.